

Sturm: Sparse Tubal-Regularized Multilinear Regression for fMRI

Wenwen Li^{*1} Jian Lou^{*2} Shuo Zhou¹ Haiping Lu¹

Abstract

While functional magnetic resonance imaging (fMRI) is important for healthcare/neuroscience applications, it is challenging to classify or interpret due to its multi-dimensional structure, high dimensionality, and small number of samples available. Recent sparse multilinear regression methods based on tensor are emerging as promising solutions for fMRI, yet existing works rely on unfolding/folding operations and a tensor rank relaxation with limited tightness. The newly proposed tensor singular value decomposition (t-SVD) sheds light on new directions. In this work, we study t-SVD for sparse multilinear regression and propose a **S**parse **t**ubal-regularized **M**ultilinear regression (**Sturm**) method for fMRI. Specifically, the Sturm model performs multilinear regression with two regularization terms: a tubal tensor nuclear norm based on t-SVD and a standard ℓ_1 norm. We further derive the algorithm under the alternating direction method of multipliers framework. We perform experiments on four classification problems, including both resting-state fMRI for disease diagnosis and task-based fMRI for neural decoding. The results show the superior performance of Sturm in classifying fMRI using just a small number of voxels.

1. Introduction

Brain diseases affect millions of people worldwide and impose significant challenges to healthcare systems. Functional magnetic resonance imaging (fMRI) is a key medical imaging technique for diagnosis, monitoring and treatment of brain diseases. Beyond healthcare, fMRI is also an indispensable tool in neuroscience studies (Faro & Mohamed, 2010).

^{*}Equal contribution ¹Department of Computer Science, University of Sheffield, UK ²Department of Computer Science, Hong Kong Baptist University, China. Correspondence to: Wenwen Li <wenwen.li@sheffield.ac.uk>, Jian Lou <loujian0425@gmail.com>, Shuo Zhou <szhou20@sheffield.ac.uk>, Haiping Lu <h.lu@sheffield.ac.uk>.

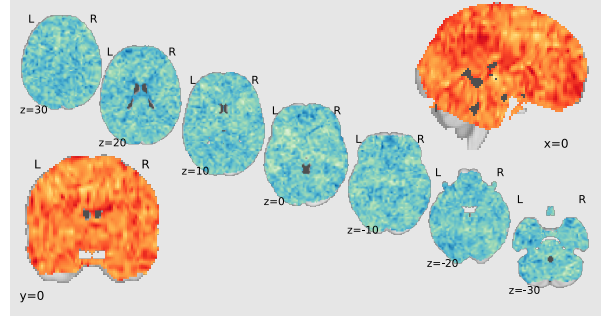


Figure 1. A 3D fMRI volume has three directions: sagittal (x), coronal (y) and axial (z). The original scans are taken with slices oriented in parallel to axial plane (as shown in the diagonal). We aim to classify fMRI with only a small number of voxels for easy interpretation by proposing a sparse multilinear regression model with tubal tensor nuclear norm regularization. (This figure is best viewed on screen.)

fMRI records the Blood Oxygenation Level Dependent (BOLD) signal caused by changes in blood flow (Ogawa et al., 1990), as depicted in Fig. 1. fMRI scan is a four-dimensional (4-D) sequence composed of magnetic resonance imaging (MRI) volumes sampled every few seconds, with over 100,000 voxels each MRI volume. It is often represented as a three-dimensional (3-D) volume, with the statistics of each voxel summarized along the time axis. Figure 1 visualizes example values of such statistics, showing very different characteristics from natural images.

Unlike natural images, fMRI data is expensive to obtain. Thus, the number of fMRI samples in a study is typically limited to dozens. This makes fMRI challenging to analyze, particularly in its full (i.e., whole brain). Moreover, in healthcare and neuroscience, prediction accuracy is not the only concern. It is also important to interpret the learned features to domain experts such as clinicians or neuroscientists. This makes sparse learning models (Ryali et al., 2010; Simon et al., 2013; Rao et al., 2013; Hastie et al., 2015) attractive because they can reveal direct dependency of a response with a small portion of input features. Therefore, tensor-based, sparse multilinear regression methods are emerging recently, where *tensor* refers to multidimensional array. For simplicity, we consider only *third-order* (i.e., 3-D) tensor in this paper.

Sparse multilinear regression models relate a predictor/feature tensor with a univariate response via a coefficient tensor, generalizing Lasso-based models (Tibshirani, 1996; Hastie et al., 2015) to tensor data. Regularization that promotes sparsity and low rankness is also generalized to the coefficient tensor. For example, the regularized multilinear regression and selection (Remurs) model (Song & Lu, 2017) incorporates a sparse regularization term, via an ℓ_1 norm, and a Tucker rank-minimization term, via a summation of the nuclear norms (SNN) of unfolded matrices. There are also CANDECOMP/PARAFAC (CP) rank-based methods (Tan et al., 2012; He et al., 2018). For example, the fast stagewise unit-rank tensor factorization (SURF) (He et al., 2018) enforces the low rankness via the CP decomposition model (Hitchcock, 1927; Harshman, 1970; Carroll & Chang, 1970), with the rank to be incrementally estimated via residual computation rather than direct minimization. And it proposes a divide-and-conquer strategy to improve efficiency and scalability with a greedy algorithm (Cormen et al., 2009). Although Remurs minimizes the Tucker rank directly, it involves unfolding/folding operations that transform tensor to/from matrix, which break some tensor structure, and SNN is not a tight convex relaxation of its target rank (Romera-Paredes & Pontil, 2013).

A new Tubal Tensor Nuclear Norm (TNN) (Zhang et al., 2014; Zhang & Aeron, 2017; Lu et al., 2016; 2018a) is recently proposed based on the *tubal rank*, which originates from the tensor singular value decomposition (t-SVD) (Kilmer et al., 2013). In tensor recovery problems, TNN guarantees the exact recovery under certain conditions. Improved performance has been observed on image/video data on tensor completion/recovery and robust tensor principal component analysis (PCA) (Zhang & Aeron, 2017; Lu et al., 2016; 2018a). In addition, TNN does not require unfolding/folding of tensor in its optimization.

In this work, we study sparse multilinear regression under the t-SVD framework for fMRI classification. The success of TNN is limited to *unsupervised* learning settings such as completion/recovery and robust PCA. To our knowledge, TNN has not been studied in a *supervised* setting yet, such as multilinear regression where the problem is not recovery given samples of a tensor but prediction of a response with a set of training tensor samples. Moreover, the targeted fMRI classification tasks have additional challenge of small sample size (relative to the feature dimension).

Our contributions are twofold: Firstly, we propose a **Sparse tubal-regularized multilinear regression (Sturm)** method that incorporates TNN regularization. Specifically, we formulate the *Sturm* model by incorporating both a TNN regularization and a sparsity regularization on the coefficient tensor. We solve the resulted *Sturm* problem using the alternating direction method of multipliers (ADMM) framework

(Boyd et al., 2011). TNN-based formulation allows efficient parameter update in the Fourier domain, which is highly parallelizable.

Our second contribution is that we evaluate Sturm and related methods on *both* resting-state and task-based fMRI classification problems, instead of only one of them as in previous works (Zhou et al., 2013b; 2014; Shi et al., 2014; Zhou et al., 2017; He et al., 2017). We use public datasets with identifiable subsets for repeatability, and examine both the classification accuracy and sparsity. The results show Sturm outperforming other state-of-the-art methods on the whole.

2. Related Work

Tensor decomposition and rank. There are three popular tensor decomposition methods and associated tensor rank definitions: **1)** The CP decomposition of a tensor is written as the summation of R rank-one tensors (Hitchcock, 1927; Harshman, 1970; Carroll & Chang, 1970), where R is the CP rank. **2)** For a 3-D tensor, the Tucker decomposition decomposes it into a core tensor and three factor matrices (De Lathauwer et al., 2000), and the *Tucker rank* is 3-tuple consisting of the rank for each mode- n unfolded matrix. **3)** The t-SVD views a 3-D tensor as a matrix of *tubes* (mode-3 vectors) oriented along the third dimension and decomposes it as circular convolutions on three tensors (Braman, 2010; Kilmer et al., 2013; Kilmer & Martin, 2011; Gleich et al., 2013). This leads to a new tensor *tubal rank* defined as the number of non-zero singular tubes. Please refer to (Zhang & Aeron, 2017; Zhang et al., 2014; Yuan & Zhang, 2016; Lu et al., 2016; 2018a; Mu et al., 2014) for more detailed discussion, e.g., on their pros and cons.

Low-rank tensor completion/recovery. Tensor completion/recovery takes a tensor with missing/noisy entries as the input and aims to recover/complete those entries. Low-rank assumption makes solving such problems feasible, and often with provable theoretical guarantees under mild conditions. The three types of tensor decomposition have their corresponding tensor completion/recovery approaches that minimize respective tensor ranks. Direct minimization of tensor rank is NP-hard (Hillar & Lim, 2013). Therefore, CP rank, Tucker rank, and tubal rank are relaxed to CP-based nuclear norm (Shi et al., 2017), the sum of matrix nuclear norm (Liu et al., 2013), and the tubal tensor nuclear norm.

Sparse and low-rank multilinear regression. Sparse and low-rank constraints have also been applied to multilinear regression problems. Multilinear regression models (Signoretto et al., 2010; Su et al., 2012; Guo et al., 2012; Zhou et al., 2013a) relate a predictor/feature tensor $\mathcal{X} \in \mathbb{R}^{I_1 \times I_2 \times I_3}$ with a univariate response y , via a coefficient tensor $\mathcal{W} \in \mathbb{R}^{I_1 \times I_2 \times I_3}$. The Remurs model (Song

Notation	Description
a	Lowercase letter denotes scalar
\mathbf{a}	Bold lowercase letter denotes vector
\mathbf{A}	Bold uppercase letter denotes matrix
\mathcal{A}	Calligraphic uppercase letter denotes tensor
$\mathcal{A} * \mathcal{B}$	t-product between tensors \mathcal{A} and \mathcal{B}
\mathcal{A}^\top	Tensor conjugate transpose of \mathcal{A}
$\mathbf{A}^{(i_3)}$	The i_3 th mode-3 (frontal) slice of \mathcal{A}
$\mathcal{A}_{\mathcal{F}}$	The discrete Fourier transform of \mathcal{A}

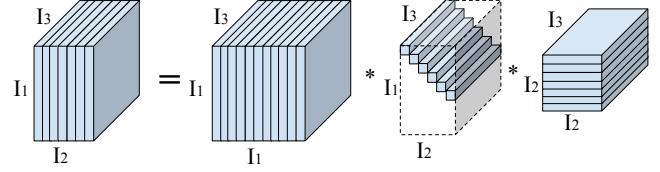
Table 1. Important notations.

& Lu, 2017) introduces regularization with a sparsity constraint, via ℓ_1 norm, and a low-rank constraint via Tucker rank-based SNN. Instead of minimizing the rank, the fast stagewise unit-rank tensor factorization (SURF) (He et al., 2018) is an efficient and scalable method that imposes a low CP rank constraint by setting a maximum rank and increasing the rank estimate from 1 to the maximum, stopping upon zero residual.

Tensor methods on fMRI. Due to the high dimensionality of fMRI data, regions of interest (ROIs) are typically used rather than all voxels in the original 3-D spatial domain (Chen et al., 2015; He et al., 2018). ROI analysis requires strong prior knowledge to determine the regions. In contrast, whole-brain fMRI analysis (Poldrack et al., 2013) is more data-driven. Thus, tensor-based machine learning methods (Cichocki, 2013; Cichocki et al., 2009) have been developed for fMRI, with promising results reported (Acar et al., 2017; Zhou et al., 2013a; Song et al., 2015; He et al., 2017; Song & Lu, 2017; Ozdemir et al., 2017; Barnathan et al., 2011). However, in these works, the learning methods are only evaluated on either resting-state fMRI for disease diagnosis (Zhou et al., 2017) or task-based fMRI for neural decoding (He et al., 2017; Chen et al., 2015; Song & Lu, 2017), but not both.

3. Tubal Tensor Nuclear Norm

Notations. Table 1 summarizes important notations used in this paper. We use lowercase, bold lowercase, bold uppercase, calligraphic uppercase letters to denote scalar, vector, matrix, and tensor, respectively. We denote indices by lowercase letters spanning the range from 1 to the uppercase letter of the index, e.g., $m = 1, \dots, M$. A third-order tensor $\mathcal{A} \in \mathbb{R}^{I_1 \times I_2 \times I_3}$ is addressed by three indices $\{i_n\}$, $n = 1, 2, 3$. Each i_n usually addresses the n th mode of \mathcal{A} , while such convention may not be strictly followed when the context is clear. The i_3 th mode-3 slice, a.k.a. the frontal slice, of \mathcal{A} is denoted as $\mathbf{A}^{(i_3)}$, a matrix obtained by fixing the mode-3 index i_3 , i.e., $\mathbf{A}^{(i_3)} = \mathcal{A}(:, :, i_3)$. The (i_1, i_2) th tube of \mathcal{A} , denoted as $\tilde{\mathbf{a}}_{i_1 i_2}$, is a mode-3 vector obtained by fixing the first two mode indices, i.e., $\mathcal{A}(i_1, i_2, :)$.


 Figure 2. Illustration of t-SVD $\mathcal{A} = \mathcal{U} * \mathcal{S} * \mathcal{V}^\top$, assuming $I_1 > I_2$.

t-SVD and tubal rank. We first review the t-SVD framework following the definitions in (Kilmer et al., 2013). The **t-product** (*tensor-tensor product*) between tensor $\mathcal{A} \in \mathbb{R}^{I_1 \times I_2 \times I_3}$ and $\mathcal{B} \in \mathbb{R}^{I_2 \times J_4 \times I_3}$ is defined as $\mathcal{A} * \mathcal{B} = \mathcal{C} \in \mathbb{R}^{I_1 \times J_4 \times I_3}$. The (i_1, j_4) th tube $\tilde{\mathbf{c}}_{i_1 j_4}$ of \mathcal{C} is computed as

$$\tilde{\mathbf{c}}_{i_1 j_4} = \mathcal{C}(i_1, j_4, :) = \sum_{i_2=1}^{I_2} \mathcal{A}(i_1, i_2, :) * \mathcal{B}(i_2, j_4, :), \quad (1)$$

where $*$ denotes the circular convolution (Rabiner & Gold, 1975) between two tubes (vectors) of the same size and the respective t-product between tensors. The **tensor conjugate transpose** of $\mathcal{A} \in \mathbb{R}^{I_1 \times I_2 \times I_3}$ is denoted as $\mathcal{A}^\top \in \mathbb{R}^{I_2 \times I_1 \times I_3}$, obtained by conjugate transposing each of the frontal slice and then reversing the order of transposed frontal slices $\mathcal{A}(:, :, i_3)$. A tensor $\mathcal{I} \in \mathbb{R}^{I \times I \times I_3}$ is an **identity tensor** if its first mode-3 slice $\mathcal{I}^{(1)}$ is an $I \times I$ identity matrix and all the rest mode-3 slices, i.e. $\mathcal{I}^{(i_3)}$ for $i_3 = 2, \dots, I_3$, are zero matrices. An **orthogonal tensor** is a tensor $\mathcal{Q} \in \mathbb{R}^{I \times I \times I_3}$ that satisfies the following condition,

$$\mathcal{Q}^\top * \mathcal{Q} = \mathcal{Q} * \mathcal{Q}^\top = \mathcal{I}, \quad (2)$$

where $\mathcal{I} \in \mathbb{R}^{I \times I \times I_3}$ is an identity tensor and $*$ is the t-product defined above. If \mathcal{A} 's all mode-3 slices $\mathbf{A}^{(i_3)}$, $i_3 = 1, \dots, I_3$ are diagonal matrices, it is called an **f-diagonal tensor**. Based on these definitions, the **t-SVD** of $\mathcal{A} \in \mathbb{R}^{I_1 \times I_2 \times I_3}$ is defined as

$$\mathcal{A} = \mathcal{U} * \mathcal{S} * \mathcal{V}^\top, \quad (3)$$

where $\mathcal{U} \in \mathbb{R}^{I_1 \times I_1 \times I_3}$, $\mathcal{V} \in \mathbb{R}^{I_2 \times I_2 \times I_3}$ are orthogonal tensors, and $\mathcal{S} \in \mathbb{R}^{I_1 \times I_2 \times I_3}$ is an f-diagonal tensor. This t-SVD definition leads to a new tensor rank, the **tubal rank**, which is defined as the number of nonzero singular tubes of \mathcal{S} , i.e. $\#\{i : \mathcal{S}(i_2, i_2, :) \neq 0\}$, assuming $I_1 \geq I_2$. Figure 2 is an illustration of t-SVD.

t-SVD via Fourier transform. t-SVD can be computed via the discrete Fourier transform (DFT) for better efficiency. We denote the Fourier transformed tensor \mathcal{A} as $\mathcal{A}_{\mathcal{F}}$, obtained via fast Fourier transform (FFT) along mode-3, i.e., $\mathcal{A}_{\mathcal{F}} = \text{fft}(\mathcal{A}, [], 3)$. The connection between t-SVD and DFT is detailed in (Kilmer et al., 2013).

Tubal Tensor nuclear norm. TNN is a convex relaxation for the tubal rank, as an average tubal multi-rank within the

unit tensor spectral norm ball (Lu et al., 2018a). It can be defined via DFT, similar to t-SVD computation above. The TNN of $\mathcal{A} \in \mathbb{R}^{I_1 \times I_2 \times I_3}$ is defined as

$$\|\mathcal{A}\|_{TNN} = \frac{1}{I_3} \sum_{i_3=1}^{I_3} \|\mathbf{A}_{\mathcal{F}}^{(i_3)}\|_*, \quad (4)$$

where $\|\cdot\|_*$ denotes the matrix nuclear norm. Please refer to (Lu et al., 2018a) for a detailed derivation and complete theoretical analysis, e.g., on the tightness of the relaxation.

Note that when $I_3 = 1$, the above definitions for tensors will be equivalent to the counterparts for matrices.

4. Sparse Multilinear Regression with Tubal Rank Regularization

Tubal rank-based TNN has shown to be superior to Tucker rank-based SNN in tensor completion/recovery (Zhang & Aeron, 2017), and tensor robust PCA (Lu et al., 2016), which are all unsupervised learning settings. To our knowledge, there is no study on TNN in a supervised learning setting yet. In this work, we explore the supervised learning with TNN and study whether TNN can improve supervised learning, e.g., multilinear regression. In the following, we propose the Sturm model and derive the Sturm algorithm under the ADMM framework.

4.1. The Sturm model

We incorporate TNN in the multilinear regression problem, which trains a model from M pairs of feature tensors and their response labels ($\mathcal{X}_m \in \mathbb{R}^{I_1 \times I_2 \times I_3}$, y_m) with $m = 1, \dots, M$ to relate them via a *coefficient tensor* $\mathcal{W} \in \mathbb{R}^{I_1 \times I_2 \times I_3}$. This can be achieved by minimizing a loss function, typically with certain regularization:

$$\min_{\mathcal{W}} \frac{1}{M} \sum_{m=1}^M L(\langle \mathcal{X}_m, \mathcal{W} \rangle, y_m) + \lambda \Omega(\mathcal{W}), \quad (5)$$

where $L(\cdot)$ is a loss function, $\Omega(\cdot)$ is a regularization function, λ is a balancing hyperparameter, and $\langle \mathcal{X}, \mathcal{W} \rangle$ denotes the inner product (a.k.a. the scalar product) of two tensors of the same size defined as

$$\langle \mathcal{X}, \mathcal{W} \rangle := \sum_{i_1} \sum_{i_2} \sum_{i_3} \mathcal{X}(i_1, i_2, i_3) \cdot \mathcal{W}(i_1, i_2, i_3), \quad (6)$$

The Remurs (Song & Lu, 2017) model uses a conventional least square loss function and assumes \mathcal{W} to be both sparse and low rank. The sparsity of \mathcal{W} is regularized by an ℓ_1 norm and the rank by an SNN norm. However, the SNN requires unfolding \mathcal{W} into matrices, susceptible to losing some higher-order structural information. Moreover, it has been pointed out in (Romera-Paredes & Pontil, 2013) that SNN is not a tight convex relaxation of its target rank.

This motivates us to propose a **Sparse tubal-regularized multilinear regression (Sturm)** model which replaces SNN in Remurs with TNN. This leads to the following objective function

$$\min_{\mathcal{W}} \frac{1}{2} \sum_{m=1}^M (y_m - \langle \mathcal{X}_m, \mathcal{W} \rangle)^2 + \tau \|\mathcal{W}\|_{TNN} + \gamma \|\mathcal{W}\|_1, \quad (7)$$

where τ and γ are hyperparameters, and $\|\mathcal{W}\|_1$ is the ℓ_1 norm of tensor \mathcal{W} , defined as

$$\|\mathcal{W}\|_1 = \sum_{i_1} \sum_{i_2} \sum_{i_3} |\mathcal{W}(i_1, i_2, i_3)|, \quad (8)$$

which is equivalent to the ℓ_1 norm of its vectorized representation \mathbf{w} . Here, the TNN regularization term $\|\mathcal{W}\|_{TNN}$ enforces low tubal rank in \mathcal{W} . The trade-off between τ and γ as well as the degenerated versions follow the analysis for the Remurs (Song & Lu, 2017).

4.2. The Sturm algorithm via ADMM

ADMM (Boyd et al., 2011) is a standard solver for Problem (7). Thus, we derive an ADMM algorithm to optimize the Sturm objective function. We begin with introducing two auxiliary variables, \mathcal{A} and \mathcal{B} to disentangle the TNN and the ℓ_1 -norm regularization:

$$\min_{\mathcal{W}} \frac{1}{2} \sum_{m=1}^M (y_m - \langle \mathcal{X}_m, \mathcal{A} \rangle)^2 + \tau \|\mathcal{B}\|_{TNN} + \gamma \|\mathcal{W}\|_1 \quad (9)$$

$$s.t. \mathcal{A} = \mathcal{W} \text{ and } \mathcal{B} = \mathcal{W}.$$

Then, we introduce two Lagrangian dual variables \mathcal{P} (for \mathcal{A}) and \mathcal{Q} (for \mathcal{B}). With a Lagrangian constant ρ , the augmented Lagrangian becomes,

$$\begin{aligned} L_{\rho}(\mathcal{A}, \mathcal{B}, \mathcal{W}, \mathcal{P}, \mathcal{Q}) &= \frac{1}{2} \sum_{m=1}^M (y_m - \langle \mathcal{X}_m, \mathcal{A} \rangle)^2 \\ &+ \tau \|\mathcal{B}\|_{TNN} + \gamma \|\mathcal{W}\|_1 \\ &+ \langle \mathcal{P}, \mathcal{A} - \mathcal{W} \rangle + \frac{\rho}{2} \|\mathcal{A} - \mathcal{W}\|_F^2 \\ &+ \langle \mathcal{Q}, \mathcal{B} - \mathcal{W} \rangle + \frac{\rho}{2} \|\mathcal{B} - \mathcal{W}\|_F^2. \end{aligned} \quad (10)$$

We further introduce two scaled dual variables $\mathcal{P}' = \frac{1}{\rho} \mathcal{P}$ and $\mathcal{Q}' = \frac{1}{\rho} \mathcal{Q}$ only for notation convenience. Next, we derive the update from iteration k to $k+1$ by taking an alternating strategy, i.e., minimizing one variable with all other variables fixed.

Updating \mathcal{A}^{k+1} :

$$\begin{aligned} \mathcal{A}^{k+1} &= \arg \min_{\mathcal{A}} L_{\rho}(\mathcal{A}, \mathcal{B}^k, \mathcal{W}^k, \mathcal{P}'^k, \mathcal{Q}'^k) \\ &= \arg \min_{\mathcal{A}} \frac{1}{2} \sum_{m=1}^M (y_m - \langle \mathcal{X}_m, \mathcal{A} \rangle)^2 + \frac{\rho}{2} \|\mathcal{A} - \mathcal{W}^k + \mathcal{P}'^k\|_F^2. \end{aligned} \quad (11)$$

Algorithm 1 Proximal Operator for TNN:
 $\text{prox}_{\mu \|\cdot\|_{TNN}}(\mathcal{T})$

Require: $\mathcal{T} \in \mathbb{R}^{I_1 \times I_2 \times I_3}, \mu$
 1: $\mathcal{T}_{\mathcal{F}} = \text{fft}(\mathcal{T}, [], 3)$;
 2: **for** $i_3 = 1, 2, \dots, I_3$ **do**
 3: $[\mathbf{U}, \text{diag}(\mathbf{s}), \mathbf{V}] = \text{svd}(\mathbf{T}_{\mathcal{F}}^{(i_3)})$
 4: $\mathbf{Z}_{\mathcal{F}}^{(i_3)} = \mathbf{U}(\text{diag}((\mathbf{s} - \mu)_+))\mathbf{V}^{\top}$;
 5: **end for**
 6: $\text{prox}_{\mu \|\cdot\|_{TNN}}(\mathcal{T}) = \text{ifft}(\mathcal{Z}_{\mathcal{F}}, [], 3)$;
Ensure: $\text{prox}_{\mu \|\cdot\|_{TNN}}(\mathcal{T})$

This can be rewritten as a linear-quadratic objective function by vectorizing all the tensors. Specifically, let $\mathbf{a} = \text{vec}(\mathcal{A})$, $\mathbf{w}^k = \text{vec}(\mathcal{W}^k)$, $\mathbf{p}^{k'} = \text{vec}(\mathcal{P}^{k'})$, $\mathbf{y} = [y_1 \cdots y_M]^{\top}$, $\mathbf{x}_m = \text{vec}(\mathcal{X}_m)$, and $\mathbf{X} = [\mathbf{x}_1 \cdots \mathbf{x}_M]^{\top}$. Then we get an equivalent objective function with the following solution:

$$\mathbf{a}^{k+1} = (\mathbf{X}^{\top} \mathbf{X} + \rho \mathbf{I})^{-1} (\mathbf{X}^{\top} \mathbf{y} + \rho (\mathbf{w}^k - \mathbf{p}^{k'})), \quad (12)$$

where \mathbf{I} is an identity matrix. Note that this does not break/lose any structure because Eq. (11) and Eq. (12) are equivalent. \mathcal{A}^{k+1} is obtained by folding (reshaping) \mathbf{a}^{k+1} into a third-order tensor, denoted as $\mathcal{A}^{k+1} = \text{tensor}_3(\mathbf{a}^{k+1})$. Here, for a fixed ρ , we can avoid high per-iteration complexity of updating \mathbf{a}^{k+1} by pre-computing a Cholesky decomposition of $(\mathbf{X}^{\top} \mathbf{X} + \rho \mathbf{I})$, which does not change over iterations.

Updating \mathcal{B}^{k+1} :

$$\begin{aligned} \mathcal{B}^{k+1} &= \arg \min_{\mathcal{B}} L_{\rho}(\mathcal{A}^{k+1}, \mathcal{B}, \mathcal{W}^k, \mathcal{P}^{k'}, \mathcal{Q}^{k'}) \\ &= \arg \min_{\mathcal{B}} \tau \|\mathcal{B}\|_{TNN} + \frac{\rho}{2} \|\mathcal{B} - \mathcal{W}^k + \mathcal{Q}^{k'}\|_F^2 \quad (13) \\ &= \text{prox}_{\frac{\tau}{\rho} \|\cdot\|_{TNN}}(\mathcal{W}^k - \mathcal{Q}^{k'}). \end{aligned}$$

This means that \mathcal{B}^{k+1} can be solved by passing parameter $\frac{\tau}{\rho}$ to the proximal operator of the TNN (Zhang et al., 2014; Zhang & Aeron, 2017). The proximal operator for the TNN at tensor \mathcal{T} with parameter μ is denoted by $\text{prox}_{\mu \|\cdot\|_{TNN}}(\mathcal{T})$ and defined as

$$\text{prox}_{\mu \|\cdot\|_{TNN}}(\mathcal{T}) := \arg \min_{\mathcal{W}} \mu \|\mathcal{W}\|_{TNN} + \frac{1}{2} \|\mathcal{W} - \mathcal{T}\|_F^2, \quad (14)$$

where $\|\cdot\|_F$ is the Frobenius norm defined as $\|\mathcal{T}\|_F = \sqrt{\langle \mathcal{T}, \mathcal{T} \rangle}$ using Eq. (6). The proximal operator for TNN can be more efficiently computed in the Fourier domain, as in Algorithm 1, where in Step 1, $(\mathbf{s} - \mu)_+ = \max\{\mathbf{s} - \mu, 0\}$ and $\text{diag}(\mathbf{a})$ denotes a diagonal matrix whose diagonal elements are from \mathbf{a} .

Algorithm 2 ADMM for Sturm

Require: (\mathcal{X}_m, y_m) for $m = 1, \dots, M$, τ , and λ ;
 1: Initialize $\mathcal{A}^0, \mathcal{B}^0, \mathcal{W}^0, \mathcal{P}^{0'}, \mathcal{Q}^{0'}$ to all zero-tensors and set ρ and K .
 2: **for** $k = 1, \dots, K$ **do**
 3: Update \mathcal{A}^{k+1} by Eq. (12);
 4: Update \mathcal{B}^{k+1} by Alg. 1 as $\text{prox}_{\frac{\tau}{\rho} \|\cdot\|_{TNN}}(\mathcal{W}^k - \mathcal{Q}^{k'})$;
 5: Update \mathcal{W}^{k+1} by Eq. (16) as

$$\text{prox}_{\frac{\gamma}{2\rho} \|\cdot\|_1} \left(\frac{\mathcal{A}^{k+1} + \mathcal{P}^{k'} + \mathcal{B}^{k+1} + \mathcal{Q}^{k'}}{2} \right);$$

 6: $\mathcal{P}^{k+1} = \mathcal{P}^{k'} + \mathcal{A}^{k+1} - \mathcal{W}^{k+1}$;
 7: $\mathcal{Q}^{k+1} = \mathcal{Q}^{k'} + \mathcal{B}^{k+1} - \mathcal{W}^{k+1}$;
 8: **end for**
Ensure: \mathcal{W}^K

Updating \mathcal{W}^{k+1} :

$$\begin{aligned} \mathcal{W}^{k+1} &= \arg \min_{\mathcal{W}} L_{\rho}(\mathcal{A}^{k+1}, \mathcal{B}^{k+1}, \mathcal{W}, \mathcal{P}^{k'}, \mathcal{Q}^{k'}) \\ &= \text{prox}_{\frac{\gamma}{2\rho} \|\cdot\|_1} \left(\frac{\mathcal{A}^{k+1} + \mathcal{P}^{k'} + \mathcal{B}^{k+1} + \mathcal{Q}^{k'}}{2} \right). \end{aligned} \quad (15)$$

It can be solved by calling the proximal operator of the ℓ_1 norm with parameter $\frac{\gamma}{2\rho}$, which is simply the element-wise soft-thresholding, i.e.

$$\text{prox}_{\mu \|\cdot\|_1}(\mathcal{T}) = (\mathcal{T} - \mu)_+. \quad (16)$$

Updating \mathcal{P}^{k+1} and \mathcal{Q}^{k+1} : The updates of \mathcal{P} and \mathcal{Q} are simply dual ascent steps:

$$\mathcal{P}^{k+1} = \mathcal{P}^{k'} + \mathcal{A}^{k+1} - \mathcal{W}^{k+1}, \quad (17)$$

$$\mathcal{Q}^{k+1} = \mathcal{Q}^{k'} + \mathcal{B}^{k+1} - \mathcal{W}^{k+1}. \quad (18)$$

The complete procedure is summarized in Algorithm 2. The code will be made publicly available via GitHub.

4.3. Computational complexity

Finally, we analyze the per-iteration computational complexity of Algorithm 2. Let $I = I_1 I_2 I_3$. Step 2 takes $O(IM + \min\{M^2, I^2\})$. Step 2 takes $O(\min\{I_1, I_2\}I)$ for the singular value thresholding in the Fourier domain, plus $O(I \log(I_3))$ for `fft` and `ifft`. Step 2 takes $O(I)$ because the proximal operation for ℓ_1 norm is element-wise. Step 2 and Step 2 take $O(I)$. As a result, in a high dimensional (or small sample) setting where $I \gg M$, the per-iteration complexity is $O(I(\log(I_3) + M))$.

5. Experiments

We evaluate our *Sturm* algorithm on four binary classification problems with six datasets from three public fMRI

repositories. While known works typically focus on either resting-state or task-based fMRI only and rarely both, here we study *both* types. We test the efficacy of the Sturm approach against five state-of-the-art algorithms and three additional variations, in terms of both classification accuracy and sparsity.

5.1. Classification problems and datasets

Resting-state fMRI for disease diagnosis. Resting-state fMRI is scanned when the subject is not doing anything, i.e., at rest. It is commonly used for brain disease diagnosis, i.e., classifying clinical population. In this paper, we consider only the binary classification of patients (positive) and health control subjects (negative).

Task-based fMRI for neural decoding. Task-based fMRI is scanned when the subject is performing certain tasks, such as viewing pictures or reading sentences (Wang et al., 2003). It is commonly used for studies decoding brain cognitive states, or neural decoding. The objective is to classify (decode) the tasks performed by subjects using the fMRI information. In this paper, we consider only binary classification of two different tasks.

Chosen datasets. We study four fMRI classification problems on six datasets from three public repositories, with the key information summarized in Table 2. Two are disease diagnosis problems on resting-state fMRI, and the other two are neural decoding problems on task-based fMRI, as described below.

- **Resting 1 – ABIDE_{NYU&UM}:** The Autism Brain Imaging Data Exchange (ABIDE)¹ (Craddock et al., 2013) consists of patients with autism spectrum disorder (ASD) and healthy control subjects. We chose the largest two subsets contributed by New York University (NYU) and University of Michigan (UM). The fMRI data has been preprocessed by the pipeline of Configurable Pipeline for the Analysis of Connectomes (CPAC). Quality control was performed by selecting the functional images with quality ‘OK’ reported in the phenotype data.
- **Resting 2 – ADHD-200_{NYU}:** We chose the NYU subset from the Attention Deficit Hyperactivity Disorder (ADHD) 200 (ADHD-200) dataset² (Bellec et al., 2017), with ADHD patients and healthy controls. The raw data is preprocessed by the pipeline of Neuroimaging Analysis Kit (NIAK).
- **Task 1 – Balloon vs Mixed gamble :** We chose two

¹http://fcon_1000.projects.nitrc.org/indi/abide

²<http://neurobureau.projects.nitrc.org/ADHD200/Data.html>

Classification Problem	# Pos.	# Neg.	Input data size $I_1 \times I_2 \times I_3$
Resting 1 – ABIDE _{NYU&UM}	101	131	61 × 73 × 61
Resting 2 – ADHD-200 _{NYU}	118	98	53 × 64 × 46
Task 1 – Balloon vs Mixed	32	32	91 × 109 × 91
Task 2 – Simon vs Flanker	42	52	91 × 109 × 91

Table 2. Summary of the four classification problems and respective datasets. # denotes the number of volumes (samples). Pos. and Neg. are short for the positive and negative classes, respectively. For diagnosis problems on ABIDE/ADHD-200, patients and health subjects are considered as positive and negative classes, respectively. The two neural decoding problems are formed by using six OpenfMRI datasets listed as Pos. vs Neg.

gamble-related datasets from the OpenfMRI repository³ (Poldrack et al., 2013) project to form a classification problem. They are 1) Balloon analog risk-taking task (BART) and 2) Mixed gambles task.

- **Task 2 – Simon vs Flanker:** We chose another two recognition and response related tasks from OpenfMRI for binary classification. They are 1) Simon task and 2) Flanker task.

Resting-state fMRI preprocessing. The raw resting-state brain fMRI data is 4-D. We follow typical approaches to reduce the 4-D data to 3-D by either taking the average (He et al., 2017) or the amplitude (Yu-Feng et al., 2007) of low frequency fluctuation of voxel values along the time dimension. We perform experiments on both and report the best results.

Task-based fMRI preprocessing. Following (Poldrack et al., 2013), we re-implemented a preprocessing pipeline to process the OpenfMRI data to obtain the 3D statistical parametric maps (SPMs) for each brain condition with a standard template. We used the same criteria as in (Poldrack et al., 2013) to selected one contrast (one specific brain condition over experimental conditions) per task for classification.

The tubal mode of fMRI. Figure 1 illustrates how fMRI scan is obtained along the axial direction, which is mode 3 in tensor representation. Each image along the diagonal is a mode-3 (frontal) slice. Therefore, it is a natural choice to consider mode 3 as the tubal mode to apply Sturm.

5.2. Algorithms

We evaluate Sturm and Sturm + SVM (support vector machine) against the following five algorithms and three additional algorithms via combination with SVM.

³Data used in this paper are available at OpenfMRI: <https://legacy.openfmri.org>, now known as OpenNeuro: <https://openneuro.org>.

- *SVM*: We chose linear SVM for both speed and prediction accuracy. (We studied both the linear and Gaussain RBF kernel SVM and found the linear one performs better on the whole.)
- *Lasso*: It is a linear regression method with the ℓ_1 norm regularization.
- *Elastic Net (ENet)*: It is a linear regression method with ℓ_1 and ℓ_2 regularization.
- *Remurs (Song & Lu, 2017)*: It is a multilinear regression model with ℓ_1 norm and Tucker rank-based SNN regularization.
- *Multi-way Multi-level Kernel Modeling (MMK) (He et al., 2017)*: It is a kernelized CP tensor factorization method to learn nonlinear features from tensors. Gaussain RBF kernel MMK is used with pre-computed kernel SVM.

SVM, Lasso, and ENet take vectorized fMRI data as input while Remurs and MMK directly take 3-D fMRI tensors as input. Lasso, ENet, Remurs, and Sturm can also be used for (embedded) feature selection. Therefore, we can add an SVM after each of them to obtain Lasso + SVM, ENet + SVM, Remurs + SVM and Sturm + SVM. The code for Sturm is built on the software library from (Lu, 2016; Lu et al., 2018b). Remurs, Lasso, and ENet are implemented with the SLEP package (Liu et al., 2009). MMK code is kindly provided by the first author of (He et al., 2017).

5.3. Algorithm and evaluation settings

Model hyperparameter tuning. Default settings are used for all existing algorithms. For Sturm, we follow the Remurs default setting (Song & Lu, 2017) to set ρ to 1 and use the same set $\{10^{-3}, 5 \times 10^{-3}, 10^{-2}, \dots, 5 \times 10^2, 10^3\}$ for τ and γ , while scaling the first term in Eq. (7) by a factor $\alpha = \sqrt{(\max(I_1, I_2) \times I_3)}$ to better balance the scales of the loss function and regularization terms (Lu et al., 2016; 2018a).

Image resizing. To improve computational efficiency and reduce the small sample size problem (and overfitting), the input 3-D tensors are further re-sized into three different sizes with a factor β , choosing from $\{0.3, 0.5, 0.7\}$.

Feature selection. In Lasso + SVM, ENet + SVM, Remurs + SVM, and Sturm + SVM, we rank the selected features by their associated absolute values of \mathcal{W} in the descending order and feed the top $\eta\%$ of the features to SVM. We study five values of η : $\{1, 5, 10, 50, 100\}$.

Evaluation metric and method. The classification accuracy is our primary evaluation metric, and we also examine the sparsity of the obtained solution for all algorithms except SVM and MMK. For a particular binary classification

problem, we perform ten-fold cross validation and report the mean and standard deviation of the classification accuracy and sparsity over ten runs. For each of the ten (test) folds, we perform an inner nine-fold cross validation using the remaining nine folds to determine τ and γ (jointly for ENet, Remurs, and Sturm on a 13×13 grid), β , and η above that give the highest classification accuracy, with the corresponding sparsity recorded. The sparsity is calculated as the ratio of the number of zeros in the output coefficient tensor \mathcal{W} to its size $I_1 \times I_2 \times I_3$. In general, higher sparsity implies better interpretability (Hastie et al., 2015).

5.4. Results and discussion

Table 3 reports the classification accuracy for all algorithms except MMK. This is because all MMK results are below 60% on all four problems, possibly due to the default settings of the CP rank and SVM kernel. (We have tried a few alternative settings without improvement, though further tuning may still lead to better results.) Table 4 presents the respective sparsity values except SVM, which uses all features so the sparsity is zero. In both tables, the best results are highlighted in **bold**, with the second best ones underlined.

Performance on Resting 1 & 2. For these two resting-state problems, Sturm + SVM has the highest accuracy of 65.45%, and Lasso is the second best with 2.45% lower accuracy. In terms of sparsity, Sturm + SVM and Sturm are the top two. Specifically, on Resting 1, Remurs + SVM and Sturm + SVM are the top two algorithms with almost identical accuracy of 64.67% and 64.66%, respectively. Moreover, Sturm + SVM also has the highest sparsity of 0.87 and Sturm has the second-highest sparsity of 0.86. For Resting 2, Sturm + SVM has outperformed all other algorithms on both accuracy (66.24%) and sparsity (0.99).

Performance on Task 1 & 2. For these two task-based problems, Sturm has outperformed all other algorithms in accuracy, with 89.10% on Task 1 and 86.89% on Task 2. Lasso is again the second best in accuracy. ENet and ENet + SVM has the best sparsity of 0.96 while their accuracy values are only 81.87% and 74.21%, respectively. Sturm + SVM has significant drop in accuracy compared with Sturm alone, and Lasso + SVM, ENet + SVM and Remurs + SVM all have lower accuracy compared to without SVM.

Summary. There are four key observations on the whole:

- Sturm has the best overall accuracy of 75.38%. Sturm has outperformed Remurs in accuracy for all four classification problems. The only difference between Sturm and Remurs is replacing SNN with TNN. Therefore, this superiority indicates that tubal rank-based TNN is superior to Tucker rank-based SNN in the supervised, regression setting.

Method	Resting 1	Resting 2	Task 1	Task 2	Average		
					Resting	Task	All
SVM	60.78 ± 0.09	63.97 ± 0.09	<u>87.38 ± 0.12</u>	82.56 ± 0.17	62.38	84.97	73.67
Lasso	61.16 ± 0.08	<u>64.84 ± 0.11</u>	<u>87.38 ± 0.12</u>	85.22 ± 0.07	63.00	86.30	74.65
ENet	61.21 ± 0.10	<u>64.38 ± 0.10</u>	81.19 ± 0.15	82.56 ± 0.17	62.80	81.87	72.34
Remurs	60.72 ± 0.08	62.13 ± 0.09	87.14 ± 0.13	<u>84.67 ± 0.15</u>	61.43	85.90	73.67
Sturm	62.05 ± 0.11	63.47 ± 0.07	89.10 ± 0.09	86.89 ± 0.16	62.76	88.00	75.38
Lasso + SVM	63.37 ± 0.08	62.56 ± 0.09	74.05 ± 0.20	72.11 ± 0.16	62.97	73.08	68.02
ENet + SVM	64.20 ± 0.07	61.61 ± 0.08	76.43 ± 0.14	72.00 ± 0.14	62.91	74.21	68.56
Remurs + SVM	64.67 ± 0.10	60.23 ± 0.10	81.19 ± 0.12	83.56 ± 0.19	62.45	82.37	72.41
Sturm+ SVM	<u>64.66 ± 0.12</u>	66.24 ± 0.06	78.10 ± 0.22	82.44 ± 0.16	65.45	80.27	72.86

Table 3. Classification accuracy (mean ± standard deviation in %). Resting 1 and Resting 2 denote two disease diagnosis problems on ABIDENYU&UM and ADHD-200, respectively. Task 1 and Task 2 denote two neural decoding problems on OpenfMRI datasets for Balloon vs Mixed gamble and Simon vs Flanker, respectively. The best accuracy among all of the compared algorithms for each column is highlighted in **bold** and the second best is underlined.

Method	Resting 1	Resting 2	Task 1	Task 2	Average		
					Resting	Task	All
Lasso	0.52 ± 0.09	0.23 ± 0.32	0.74 ± 0.12	0.73 ± 0.01	0.38	0.73	0.55
ENet	0.60 ± 0.01	0.01 ± 0.01	0.96 ± 0.05	0.95 ± 0.03	0.31	0.96	0.63
Remurs	0.69 ± 0.03	0.73 ± 0.17	0.81 ± 0.08	0.81 ± 0.07	0.71	0.81	0.76
Sturm	<u>0.86 ± 0.18</u>	<u>0.86 ± 0.24</u>	0.72 ± 0.24	<u>0.60 ± 0.15</u>	<u>0.86</u>	0.66	<u>0.76</u>
Lasso + SVM	0.57 ± 0.05	0.19 ± 0.40	0.77 ± 0.10	0.75 ± 0.06	0.38	0.76	0.57
ENet + SVM	0.58 ± 0.09	0.02 ± 0.01	0.96 ± 0.04	0.95 ± 0.04	0.30	0.96	0.63
Remurs + SVM	0.70 ± 0.13	0.74 ± 0.17	0.80 ± 0.04	0.79 ± 0.13	0.72	0.79	0.76
Sturm + SVM	0.87 ± 0.07	0.99 ± 0.01	<u>0.85 ± 0.14</u>	0.56 ± 0.11	0.93	0.71	0.82

Table 4. Sparsity (mean ± standard deviation) for respective results in Table 3 with the **best** and second best highlighted.

- The reported sparsity corresponds to the best solution determined via nine-fold cross validation. Lasso and Lasso + SVM have the lowest, i.e., poorest, sparsity. ENet and ENet + SVM also have much lower sparsity than Remurs/Sturm and their + SVM versions, more than 0.10 (10%) lower. On the other hand, ENet and ENet + SVM have the highest sparsity on task-based fMRI while getting a solution closely to zero sparsity on Resting 2, showing high variation.
- Performing SVM after the four regression methods can improve the classification accuracy (though not always) on resting-state fMRI, while it has degraded their classification performance on task-based fMRI in all cases. In particular, Lasso + SVM and Sturm + SVM on Task 1, and Lasso + SVM and ENet + SVM on Task 2 have dropped more than 10% in accuracy.
- Disease diagnosis on resting-state fMRI is significantly more challenging than neural decoding on task-based fMRI. Although it should be aware from Table 2 that the number of samples is different for the resting-state and task-based fMRI, engaged brain activities are generally easier to classify than those not engaged and the difference is consistent with results reported in the literature.

5.5. Analysis

Hyperparameter sensitivity. Figure 3 illustrates the classification performance sensitivity of Sturm on its two hyperparameters τ and γ for two problems: Resting 2 and Task 2. In general, the lower right, i.e., large τ and small γ values, shows higher accuracy. This implies that the tubal rank regularization helps more in improving the accuracy than sparsity regularization. However, Fig. 3a shows poorer smoothness than Fig. 3b, another indication of resting-state fMRI being more challenging than task-based fMRI. This makes hyperparameter tuning more difficult for resting-state fMRI, (partly) causing the poorer classification performance than task-based fMRI.

Convergence analysis. Figure 4 shows the convergence of \mathcal{W} and the Sturm objective function value in (7) on Resting 2 and Task 2. It can be seen that \mathcal{W} has a fast convergence speed in both cases, though the objective function converges at a slower rate.

6. Conclusion

In this paper, we proposed a sparse tubal rank regularized multilinear regression model (*Sturm*). It performs regression with penalties on the tubal tensor nuclear norm, a convex

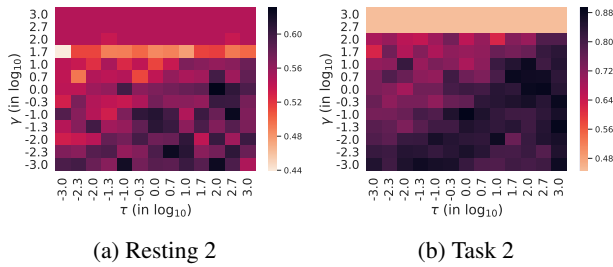


Figure 3. Sensitivity study on hyperparameters τ and γ . Darker color indicates better classification accuracy (best viewed on screen).

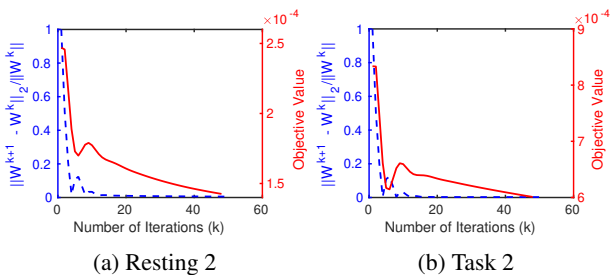


Figure 4. Convergence analysis (best viewed on screen).

relaxation of the tubal rank, and the standard ℓ_1 norm. To the best of our knowledge, this is the first supervised learning method using TNN. The Sturm algorithm is derived via a standard ADMM framework.

We evaluated Sturm (and Sturm + SVM) in terms of classification accuracy and sparsity against eight other methods on four binary classification problems from three public fMRI repositories. The datasets include both resting-state and task-based fMRI, unlike most existing works focusing on only one of them. The results showed the superior overall performance of Sturm (and Sturm + SVM in some cases) over other methods and confirmed the benefits of TNN and tubal rank regularization in a supervised setting.

References

Acar, Evrim, Levin-Schwartz, Yuri, Calhoun, Vince D, and Adali, Tülay. Tensor-based fusion of eeg and fmri to understand neurological changes in schizophrenia. In *Circuits and Systems (IS-CAS), 2017 IEEE International Symposium on*, pp. 1–4. IEEE, 2017.

Barnathan, Michael, Megalooikonomou, Vasileios, Faloutsos, Christos, Faro, Scott, and Mohamed, Feroze B. Twave: High-order analysis of functional mri. *Neuroimage*, 58(2):537–548, 2011.

Bellec, Pierre, Chu, Carlton, Chouinard-Decorte, Francois, Benhajali, Yassine, Margulies, Daniel S, and Craddock, R Cameron. The neuro bureau adhd-200 preprocessed repository. *Neuroimage*, 144:275–286, 2017.

Boyd, Stephen, Parikh, Neal, Chu, Eric, Peleato, Borja, Eckstein, Jonathan, et al. Distributed optimization and statistical learning via the alternating direction method of multipliers. *Foundations and Trends® in Machine Learning*, 3(1):1–122, 2011.

Braman, Karen. Third-order tensors as linear operators on a space of matrices. *Linear Algebra and its Applications*, 433(7):1241–1253, 2010.

Carroll, J Douglas and Chang, Jih-Jie. Analysis of individual differences in multidimensional scaling via an n-way generalization of eckart-young decomposition. *Psychometrika*, 35(3): 283–319, 1970.

Chen, Po-Hsuan Cameron, Chen, Janice, Yeshurun, Yaara, Hasson, Uri, Haxby, James, and Ramadge, Peter J. A reduced-dimension fmri shared response model. In *Advances in Neural Information Processing Systems*, pp. 460–468, 2015.

Cichocki, Andrzej. Tensor decompositions: a new concept in brain data analysis? *arXiv preprint arXiv:1305.0395*, 2013.

Cichocki, Andrzej, Zdunek, Rafal, Phan, Anh Huy, and Amari, Shun-ichi. *Nonnegative matrix and tensor factorizations: applications to exploratory multi-way data analysis and blind source separation*. John Wiley & Sons, 2009.

Cormen, Thomas H, Leiserson, Charles E, Rivest, Ronald L, and Stein, Clifford. *Introduction to algorithms*. MIT press, 2009.

Craddock, Cameron, Benhajali, Yassine, Chu, Carlton, Chouinard, Francois, Evans, Alan, Jakab, András, Khundrakpam, Budhachandra S, Lewis, John D, Li, Qingyang, Milham, Michael, et al. The neuro bureau preprocessing initiative: open sharing of preprocessed neuroimaging data and derivatives. *Neuroinformatics*, 2013.

De Lathauwer, Lieven, De Moor, Bart, and Vandewalle, Joos. A multilinear singular value decomposition. *SIAM journal on Matrix Analysis and Applications*, 21(4):1253–1278, 2000.

Faro, Scott H and Mohamed, Feroze B. *BOLD fMRI: A guide to functional imaging for neuroscientists*. Springer Science & Business Media, 2010.

Gleich, David F, Greif, Chen, and Varah, James M. The power and arnoldi methods in an algebra of circulants. *Numerical Linear Algebra with Applications*, 20(5):809–831, 2013.

Guo, W., Kotsia, I., and Patras, I. Tensor learning for regression. *IEEE Trans. on Image Processing*, 21(2):816–827, 2012.

Harshman, Richard A. Foundations of the parafac procedure: Models and conditions for an “explanatory” multimodal factor analysis. 1970.

Hastie, Trevor, Tibshirani, Robert, and Wainwright, Martin. *Statistical learning with sparsity: the lasso and generalizations*. CRC press, 2015.

He, Lifang, Lu, Chun-Ta, Ding, Hao, Wang, Shen, Shen, Linlin, Philip, S Yu, and Ragin, Ann B. Multi-way multi-level kernel modeling for neuroimaging classification. In *Computer Vision and Pattern Recognition (CVPR), 2017 IEEE Conference on*, pp. 6846–6854. IEEE, 2017.

He, Lifang, Chen, Kun, Xu, Wanwan, Zhou, Jiayu, and Wang, Fei. Boosted sparse and low-rank tensor regression. In *Advances in Neural Information Processing Systems 31*, 2018.

- Hillar, Christopher J and Lim, Lek-Heng. Most tensor problems are np-hard. *Journal of the ACM (JACM)*, 60(6):45, 2013.
- Hitchcock, Frank L. The expression of a tensor or a polyadic as a sum of products. *Journal of Mathematics and Physics*, 6(1-4): 164–189, 1927.
- Kilmer, Misha E and Martin, Carla D. Factorization strategies for third-order tensors. *Linear Algebra and its Applications*, 435(3):641–658, 2011.
- Kilmer, Misha E, Braman, Karen, Hao, Ning, and Hoover, Randy C. Third-order tensors as operators on matrices: A theoretical and computational framework with applications in imaging. *SIAM Journal on Matrix Analysis and Applications*, 34(1):148–172, 2013.
- Liu, J., Musialski, P., Wonka, P., and Ye, J. Tensor completion for estimating missing values in visual data. *IEEE Trans. on Pattern Analysis and Machine Intelligence*, 35(1):208–220, 2013.
- Liu, Jun, Ji, Shuiwang, Ye, Jieping, et al. Slep: Sparse learning with efficient projections. *Arizona State University*, 6(491):7, 2009.
- Lu, Canyi. *A Library of ADMM for Sparse and Low-rank Optimization*. National University of Singapore, June 2016. <https://github.com/canyilu/LibADMM>.
- Lu, Canyi, Feng, Jiashi, Chen, Yudong, Liu, Wei, Lin, Zhouchen, and Yan, Shuicheng. Tensor robust principal component analysis: Exact recovery of corrupted low-rank tensors via convex optimization. In *Proceedings of the IEEE Conference on Computer Vision and Pattern Recognition*, pp. 5249–5257, 2016.
- Lu, Canyi, Feng, Jiashi, Chen, Yudong, Liu, Wei, Lin, Zhouchen, and Yan, Shuicheng. Tensor robust principal component analysis with a new tensor nuclear norm. *arXiv preprint arXiv:1804.03728*, 2018a.
- Lu, Canyi, Feng, Jiashi, Yan, Shuicheng, and Lin, Zhouchen. A unified alternating direction method of multipliers by majorization minimization. *IEEE Transactions on Pattern Analysis and Machine Intelligence*, 40(3):527–541, 2018b.
- Mu, Cun, Huang, Bo, Wright, John, and Goldfarb, Donald. Square deal: Lower bounds and improved relaxations for tensor recovery. In *International Conference on Machine Learning*, pp. 73–81, 2014.
- Ogawa, Seiji, Lee, Tso-Ming, Kay, Alan R, and Tank, David W. Brain magnetic resonance imaging with contrast dependent on blood oxygenation. *Proceedings of the National Academy of Sciences*, 87(24):9868–9872, 1990.
- Ozdemir, Alp, Villafane-Delgado, Marisel, Zhu, David C, Iwen, Mark A, and Aviyente, Selin. Multi-scale higher order singular value decomposition (ms-hosvd) for resting-state fmri compression and analysis. In *Acoustics, Speech and Signal Processing (ICASSP), 2017 IEEE International Conference on*, pp. 6299–6303. IEEE, 2017.
- Poldrack, Russell A, Barch, Deanna M, Mitchell, Jason, Wager, Tor, Wagner, Anthony D, Devlin, Joseph T, Cumba, Chad, Koyejo, Oluwasanmi, and Milham, Michael. Toward open sharing of task-based fMRI data: the OpenfMRI project. *Frontiers in Neuroinformatics*, 7:12, 2013.
- Rabiner, Lawrence R and Gold, Bernard. Theory and application of digital signal processing. *Englewood Cliffs, NJ, Prentice-Hall, Inc., 1975. 777 p.*, 1975.
- Rao, Nikhil, Cox, Christopher, Nowak, Rob, and Rogers, Timothy T. Sparse overlapping sets lasso for multitask learning and its application to fmri analysis. In *Advances in neural information processing systems*, pp. 2202–2210, 2013.
- Romera-Paredes, Bernardino and Pontil, Massimiliano. A new convex relaxation for tensor completion. In *Advances in Neural Information Processing Systems*, pp. 2967–2975, 2013.
- Ryali, Srikanth, Supekar, Kaustubh, Abrams, Daniel A, and Menon, Vinod. Sparse logistic regression for whole-brain classification of fmri data. *NeuroImage*, 51(2):752–764, 2010.
- Shi, Qiquan, Lu, Haiping, and Cheung, Yiu-ming. Tensor rank estimation and completion via cp-based nuclear norm. In *Proceedings of the 2017 ACM on Conference on Information and Knowledge Management*, pp. 949–958. ACM, 2017.
- Shi, Yinghuan, Suk, Heung-II, Gao, Yang, and Shen, Dinggang. Joint coupled-feature representation and coupled boosting for ad diagnosis. In *Proceedings of the IEEE Conference on Computer Vision and Pattern Recognition*, pp. 2721–2728, 2014.
- Signoretto, Marco, De Lathauwer, Lieven, and Suykens, Johan AK. Nuclear norms for tensors and their use for convex multilinear estimation. *Submitted to Linear Algebra and Its Applications*, 43, 2010.
- Simon, Noah, Friedman, Jerome, Hastie, Trevor, and Tibshirani, Robert. A sparse-group lasso. *Journal of Computational and Graphical Statistics*, 22(2):231–245, 2013.
- Song, Xiaonan and Lu, Haiping. Multilinear regression for embedded feature selection with application to fmri analysis. In *AAAI*, pp. 2562–2568, 2017.
- Song, Xiaonan, Meng, Lingnan, Shi, Qiquan, and Lu, Haiping. Learning tensor-based features for whole-brain fmri classification. In *International Conference on Medical Image Computing and Computer-Assisted Intervention*, pp. 613–620. Springer, 2015.
- Su, Ya, Gao, Xinbo, Li, Xuelong, and Tao, Dacheng. Multivariate multilinear regression. *IEEE Transactions on Systems, Man, and Cybernetics, Part B (Cybernetics)*, 42(6):1560–1573, 2012.
- Tan, Xu, Zhang, Yin, Tang, Siliang, Shao, Jian, Wu, Fei, and Zhuang, Yueting. Logistic tensor regression for classification. In *International Conference on Intelligent Science and Intelligent Data Engineering*, pp. 573–581. Springer, 2012.
- Tibshirani, Robert. Regression shrinkage and selection via the lasso. *Journal of the Royal Statistical Society. Series B (Methodological)*, pp. 267–288, 1996.
- Wang, Xuerui, Mitchell, Tom M, and Hutchinson, Rebecca. Using machine learning to detect cognitive states across multiple subjects. *CALD KDD project paper*, 2003.
- Yu-Feng, Zang, Yong, He, Chao-Zhe, Zhu, Qing-Jiu, Cao, Man-Qiu, Sui, Meng, Liang, Li-Xia, Tian, Tian-Zi, Jiang, and Yu-Feng, Wang. Altered baseline brain activity in children with adhd revealed by resting-state functional mri. *Brain and Development*, 29(2):83–91, 2007.

- Yuan, Ming and Zhang, Cun-Hui. On tensor completion via nuclear norm minimization. *Foundations of Computational Mathematics*, 16(4):1031–1068, 2016.
- Zhang, Zemin and Aeron, Shuchin. Exact tensor completion using t-svd. *IEEE Transactions on Signal Processing*, 65(6):1511–1526, 2017.
- Zhang, Zemin, Ely, Gregory, Aeron, Shuchin, Hao, Ning, and Kilmer, Misha. Novel methods for multilinear data completion and de-noising based on tensor-svd. In *Proceedings of the IEEE Conference on Computer Vision and Pattern Recognition*, pp. 3842–3849, 2014.
- Zhou, Hua, Li, Lexin, and Zhu, Hongtu. Tensor regression with applications in neuroimaging data analysis. *Journal of the American Statistical Association*, 108(502):540–552, 2013a.
- Zhou, Luping, Wang, Lei, Liu, Lingqiao, Ogunbona, Philip, and Shen, Dinggang. Discriminative brain effective connectivity analysis for alzheimer’s disease: a kernel learning approach upon sparse gaussian bayesian network. In *Proceedings of the IEEE Conference on Computer Vision and Pattern Recognition*, pp. 2243–2250, 2013b.
- Zhou, Luping, Wang, Lei, and Ogunbona, Philip. Discriminative sparse inverse covariance matrix: application in brain functional network classification. In *Proceedings of the IEEE Conference on Computer Vision and Pattern Recognition*, pp. 3097–3104, 2014.
- Zhou, Luping, Wang, Lei, Zhang, Jianjia, Shi, Yinghuan, and Gao, Yang. Revisiting metric learning for spd matrix based visual representation. In *Proceedings of the IEEE Conference on Computer Vision and Pattern Recognition (CVPR)*, pp. 3241–3249, 2017.